AD NUMBER
AD463164
LIMITATION CHANGES

TO:

Approved for public release; distribution is unlimited.

FROM:

Distribution authorized to U.S. Gov't. agencies and their contractors; Administrative/Operational Use; JAN 1965. Other requests shall be referred to Defense Advanced Research Projects Agency, 3701 North Fairfax Drive, Arlington, VA 22203-1714.

AUTHORITY

mit/ll ltr, 2 May 1966

Technical Report

375

W. M. Kornegay

Production and Propagation of Spherical Shock Waves at Low Ambient Pressures

26 January 1965

MASSACHUSETTS INSTITUTE OF TECHNOLOGY

LINCOLN LABORATORY

PRODUCTION AND PROPAGATION OF SPHERICAL SHOCK WAVES AT LOW AMBIENT PRESSURES
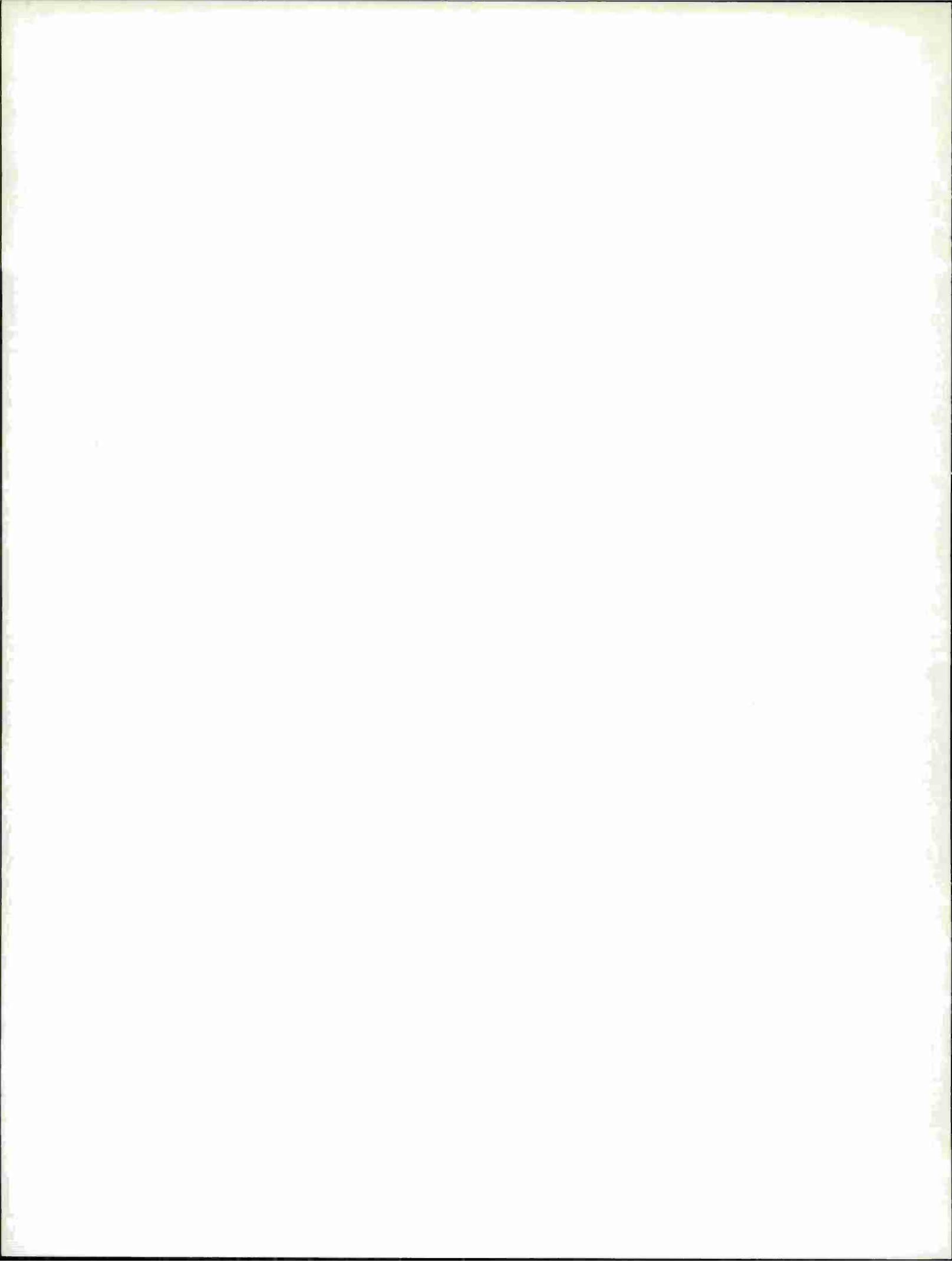
W. M. KORNEGAY

Group 35

TECHNICAL REPORT 375

26 JANUARY 1965

LEXINGTON   MASSACHUSETTS

ABSTRACT

An experimental investigation has been made of the spherical shock waves produced when 2-cm-diameter thin-walled glass spheres, which have been filled with air at a pressure of about 760 torrs, are burst in an ambient environment of dry air at pressures ranging from 0.015 to 5.0 torrs.

Piezoelectric pressure transducers were used to measure the rate of decay of the spherical-shock Mach number with increasing radius. A comparison of the experimentally observed shock Mach numbers with those predicted from calculations based on an approximate theory by Friedman and Whitham shows that the two are in good agreement. Shock overpressures and shock thickness determined from impact pressure records are in fair agreement with existing approximate theories.

The effect of glass particles on the flow field was found to be important when the initial pressure ratio across the glass diaphragm is below 500. At low pressures, viscous and rarefied flow phenomena tend to cause the measured impact pressure to depart radically from the theoretical value for continuum flow.

TABLE OF CONTENTS

PRODUCTION AND PROPAGATION OF SPHERICAL SHOCK WAVES AT LOW AMBIENT PRESSURES

I. INTRODUCTION

The study of spherical flow fields in the laboratory has been far less extensive than the study of one-dimensional flow. To the writer's knowledge, the results presented by Boyer, et al.,[1] Boyer,[2] and Glass[3] for the production of spherical shock waves by shattering pressurized glass spheres are the only available experimental data on spherical flows which have been obtained under carefully controlled laboratory conditions. The techniques used by Boyer, et al.,[1] and Boyer[2] were suitable for the production and study of spherical flows in a gas near atmospheric pressure. Some of the techniques, e.g., the application of high-speed schlieren photography to the study of the spherical flow field, cannot be used successfully at pressures below about 10 torrs.

Glass[3] concludes that pressurized glass spheres might have useful application for spherical flow studies in a rarefied atmosphere. The major advantage in the application of pressurized glass spheres to shock wave studies in a rarefied atmosphere is that the investigation will not be complicated by the presence of viscous boundary layer interference, which always exists in one-dimensional flow produced in a shock tube.

The present experimental investigation was undertaken with three objectives:

(a) To determine whether reproducible spherical flows at ambient pressures well below 1 atmos could be generated by the controlled shattering of small, thin-walled glass spheres which are filled approximately to atmospheric pressure.

(b) To compare the strength of the main shock wave with an existing theory which assumes that the decrease in shock strength with increasing shock radius is mainly due to the increased shock surface area.

(c) To study the effects of rarefied flow phenomena on impact pressure measurements.

II. REVIEW OF PREVIOUS WORK

A. Experiments at UTIA

About five years ago Boyer, et al.,[1] and Boyer[2] at the University of Toronto Institute of Aerophysics performed experimental investigations in which they studied the spherical flow generated by the shattering of 1-, 2-, and 5-inch-diameter pressurized glass spheres. The spheres were filled with air or helium at pressures between 10 and 22 atmos and were usually exploded in air at atmospheric pressure. The spheres were exploded into a 3-foot-diameter steel sphere and were shattered by a solenoid-actuated spring-loaded mallet.

High-speed schlieren and spark shadowgraph photography were used to record the explosion phenomena. Limited pressure records of the reflection of the spherical shock wave at several radii were also made. The experiments yielded results which were in good agreement with the predictions of theory, as computed with Brode's numerical solution (Sec. II-B) to the equations of motion and state.

B. Brode's Theoretical Work

Finding the solution of the set of nonlinear, partial differential equations representing the conservation of mass, momentum, and energy is the key to describing the gas dynamics of the spherically symmetric flow which results from the release of a high-pressure sphere of gas into a surrounding environment at a lower pressure. Since the set of differential equations is too difficult to solve in closed form, one often resorts to numerical techniques.

Using a method proposed by von Neumann and Richtmyer,[4] Brode[5] numerically solved the conservation equations for a spherically symmetric flow produced by a finite source explosion. Brode began by formulating the conservation equations in Lagrangian coordinates. He then proceeded to approximate the equations by a set of stable finite-difference equations. A solution of the flow equations for a specific set of initial and boundary conditions was then obtained from a numerical integration of the finite-difference equations. For any real problem, an electronic computer is needed to perform the extensive numerical calculation. In the Brode analysis, an artificial viscosity was introduced for the purpose of spreading the shock wave into a thin, continuous transition. The artificial viscosity removes the danger of complications which would result from shock discontinuities.

Details on the finite-difference equations, the boundary conditions, and the required stability conditions that Brode used to obtain the numerical solution to the partial differential equations of motion and state are given in Ref. 4. The application of Brode's numerical method to solving the spherical flow problem produced by a blast from a pressurized sphere is presented in Ref. 2. A comparison is made between the computational and experimental results.

C. Friedman-Whitham Shock Area Relation

Whitham[6] and Chisnell,[7] working independently, have recently developed techniques in shock dynamics for obtaining a differential equation for the motion of a shock wave. The equation gives the relation between changes in shock strength and channel area for the case of a shock wave moving through a channel with a varying cross-sectional area. Friedman[8] extended Whitham's work by integrating the differential equation and obtaining an analytic expression in closed form. The combined result of these efforts will be referred to as the Friedman-Whitham theory throughout this report.

Since the experimental data presented in this report will be compared with the Friedman-Whitham theory, some of the details of this theory and the derivation of the equations describing the shock motion will be presented now. The equation of motion which is valid along positive characteristics is written in characteristic form:

$$dP + \rho a \, du = -\rho \, \frac{a^2 u}{u + a} \, \frac{dA}{A} \tag{1}$$

where ρ, P, a, u, and A denote density, pressure, sound speed, particle velocity, and tube cross-sectional area, respectively. This differential relation, which is satisfied by flow

2

quantities along characteristics coming into the shock, is then applied to the flow quantities just behind the shock wave. The latter flow quantities are given in terms of the shock Mach number (M = shock velocity/a_1, where a_1 is the sound speed of gas ahead of the shock) by the Rankine-Hugoniot relations. At the shock front, these relations are

$$u = \frac{2a_1}{\gamma + 1} (M - M^{-1})$$

$$\rho = \rho_1 \frac{M^2(\gamma + 1)}{M^2(\gamma - 1) + 2}$$

$$P = \frac{\rho_1 a_1^2}{\gamma(\gamma + 1)} (2\gamma M^2 - \gamma + 1)$$

$$a^2 = a_1^2 (2\gamma M^2 - \gamma + 1) \frac{M^2(\gamma - 1) + 2}{[M(\gamma + 1)]^2}$$

where the subscript 1 denotes values ahead of the shock wave. The substitution of these expressions into Eq. (1) yields the relation

$$-\frac{dA}{A} = \frac{2MdM}{(M^2 - 1) K(M)} \tag{2}$$

where

$$K(M) = \frac{2}{\left(1 + \frac{2}{\gamma + 1} \frac{1 - x^2}{x}\right) (2x + 1 + M^{-2})}$$

$$x^2 = \frac{(\gamma - 1) M^2 + 2}{2\gamma M^2 - \gamma + 1}$$

and γ is the specific heat ratio. By identifying the channel area in Eq. (2) with the shock surface area, a differential equation which gives changes in shock Mach number as a function of the spherical shock radius R is obtained

$$-\frac{dR}{R} = \frac{MdM}{(M^2 - 1) K(M)} \quad . \tag{3}$$

This differential equation can be integrated to give the explicit formula

$$\left(\frac{R}{R_o}\right)^2 \frac{(Y - Z)^2}{M} [(\gamma - 1)^{1/2} Y + (2\gamma)^{1/2} Z]^{(2\gamma/\gamma - 1)^{1/2}} Y^{2/\gamma}$$

$$\times \exp \left\{ (2\gamma - 2)^{-1/2} \sin^{-1} \left[\frac{2Y^2 - (\gamma - 1) Z^2}{(\gamma + 1)^2 M^2} \right] \right\} = C \tag{4}$$

where

$$Y^2 = 2\gamma M^2 - \gamma + 1$$

$$Z^2 = (\gamma - 1) M^2 + 2$$

C is the constant of integration, and R_o is the radius of the unruptured high-pressure gas sphere.

When the initial conditions that specify the position and Mach number of the main shock wave at the instant the diaphragm separating the low- and high-pressure gas is ruptured are known,

Eq. (4) can be used to describe the shock motion which results from the expansion of an isothermal high-pressure sphere of gas into ambient gas at a lower pressure. These initial conditions can be determined by use of one-dimensional shock tube theory. The shock wave Mach number M_o at the point $R/R_o = 1$ and $t = 0$ is determined from the relation:

$$\frac{P_4}{P_1} \left[1 - \frac{a_1}{a_4} \frac{\gamma_4 - 1}{\gamma_1 + 1} (M_o - M_o^{-1}) \right]^{2\gamma_4/\gamma_4 - 1} = \frac{2\gamma_1 M_o^2 - \gamma_1 + 1}{\gamma_1 + 1} \tag{5}$$

where P is the pressure and the other symbols have the meaning assigned to them above. The subscript 4 refers to values in the unruptured high-pressure sphere (state 4 in Fig. 3), and the subscript 1 refers to values in the surrounding gas into which the main shock propagates (state 1 of Fig. 3). The constant of integration is then determined by setting $M = M_o$ and $R/R_o = 1$ in Eq. (4). This puts Eq. (4) in a form that permits one to compute the shock Mach number at any radius greater than $R/R_o = 1$.

A plot of Eq. (5) for air ($\gamma_4 = \gamma_1 = 1.4$) is given in Fig. 1. [The solid curves of Fig. 10(a-g) show plots of Eq. (4) at several initial Mach numbers.]

It must be emphasized that the Friedman-Whitham method for determining the strength of the main shock wave as a function of its location is based on its spherical geometry and initial strength. The weakening effect of disturbances, which originate in the flow field behind the shock wave and overtake it, is neglected. It is expected that the accuracy of the theory in predicting the motion of the main shock wave will increase with increasing initial shock Mach number, since the likelihood that weakening disturbances will overtake the shock wave decreases.

Friedman has compared the results obtained by using the Brode theory with those obtained by using the Friedman-Whitham theory for a spherical flow field having an initial Mach number
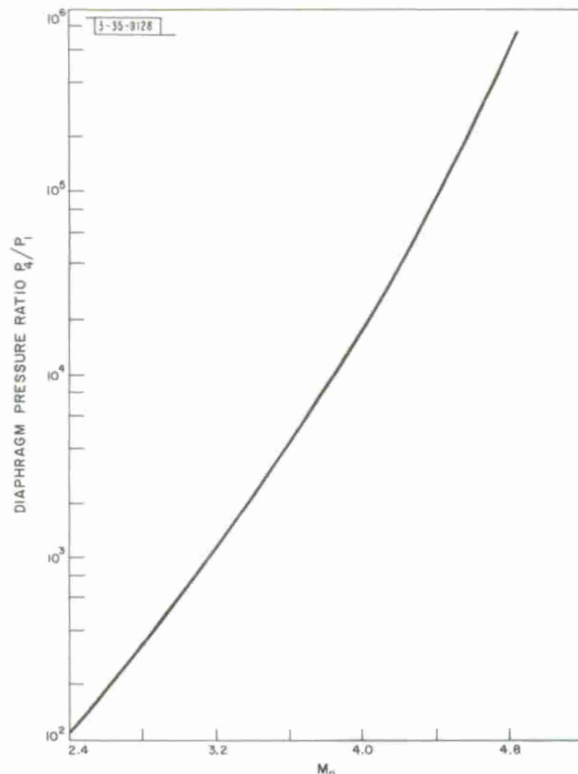

Fig. 1. Variation of initial shock Mach number in air with diaphragm pressure ratio.

4

of 1.85. He found that the initial motion of the main shock wave, as described by the two theories, was approximately the same. This suggests that the main shock weakens mainly because of its increased surface area and that the Friedman-Whitham spherical shock relation [Eq. (4)] is indeed a good approximation to the solution of the complete spherical flow field equations. The experimental results presented in this report will be used to test this theory further.

III. DESCRIPTION OF THE SPHERICAL FLOW FIELD

Theoretical and experimental studies[1,2,5,8] of the gas dynamics which result from the sudden release of spherically symmetric finite sources of high-pressure gases show that the spherical flow process is characterized by the following general features:

(a) Immediately after removing the diaphragm, a spherical shock wave is generated and moves out into the surrounding gas.

(b) There is a formation decrement associated with the spherical shock wave which is similar to that in the development of a plane shock wave in a conventional shock tube.

(c) The pressure is at a maximum immediately behind the main shock wave and falls off continuously with increasing distance behind the shock front.

(d) Because of the three dimensionality of the flow, the shock wave decelerates as it moves out radially.

(e) A steady-state region in the flow field, such as the uniform region existing between the shock wave and contact surface in a conventional shock tube, does not exist.

(f) The high-pressure gas is expanded through a spherical rarefaction wave.

(g) A contact front separates the expanded sphere gas from the surrounding gas which has been traversed by the shock wave.

(h) The contact surface initially moves outward behind the main shock wave but with a continually decreasing velocity.

(i) A second shock wave which has its origin at the tail of the rarefaction wave exists in the flow field; this shock wave moves inward initially and then moves outward, but it never overtakes the main shock wave.

It is thus apparent that the spherical flow which results when a sphere of gas, at a pressure higher than that of the surrounding gas, is released suddenly is similar in many ways to the flow in a conventional shock tube. One of the chief differences is pointed out in Fig. 2 which shows the pressure profiles immediately behind the main shock waves in the one-dimensional and the three-dimensional flow fields. In this figure, P_1 is the pressure ahead of the shock wave, and P_2 is the pressure behind the shock wave.

The history of the spherical flow is presented schematically in Fig. 3 which shows the space-time loci of the waves at a time t after the shock is initiated. In Fig. 3, state 1 is at low pressure and is the gas into which the main shock propagates; state 4 is the undisturbed gas initially contained behind the diaphragm at a pressure higher than state 1; state 2 is gas, originally in state 1, that has been compressed and heated irreversibly; state 5 is gas, originally in state 4, that has been expanded by the rarefaction wave; state 3 is gas, originally in state 4, that has been expanded by the rarefaction wave and then compressed by the second shock wave.

States 2 and 3 are separated by a contact surface. A secondary shock wave separates states 3 and 5. From the flow diagram of Fig. 3, one notices that all the wave elements, except the head of the rarefaction wave, are curved in the distance-time plane. A similar flow diagram for one-dimensional flow would show that all wave elements are straight and that the second shock wave does not exist.
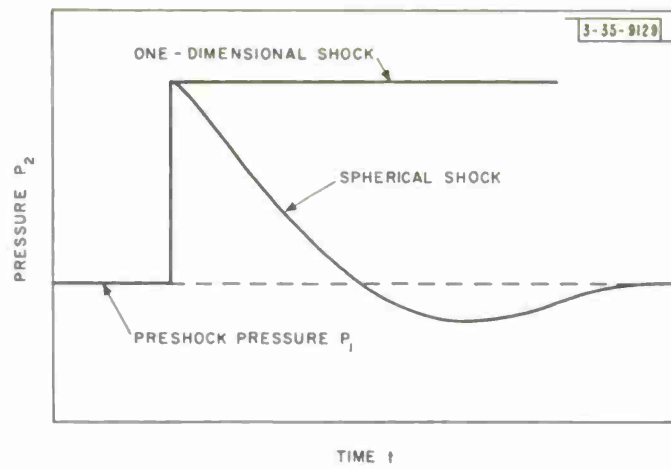
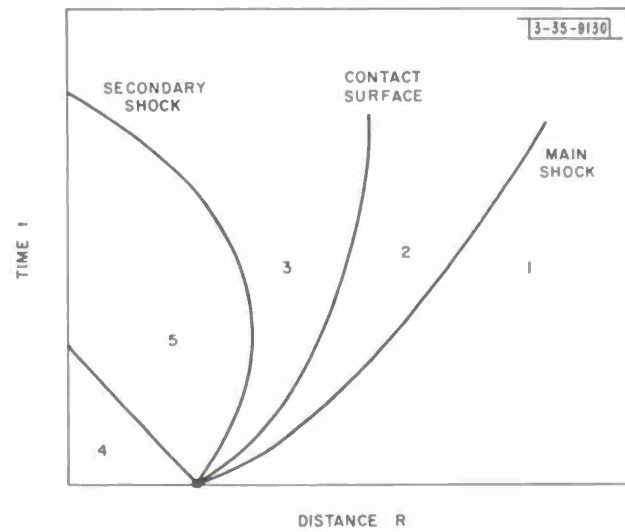Fig. 2. Pressure profiles behind one-dimensional and spherical shock waves.

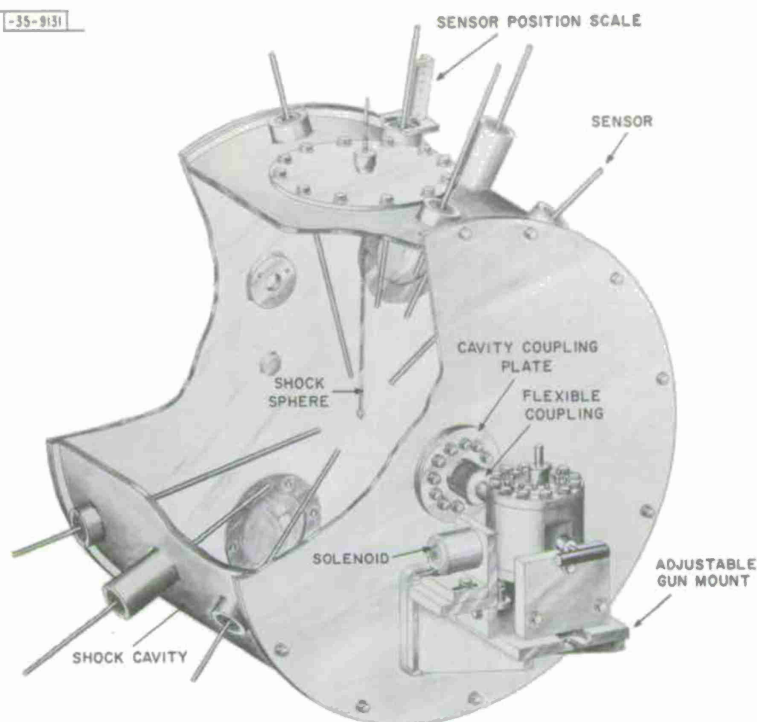Fig. 3. Distance vs time for spherical flow field.

Fig. 4. Schematic of shock cavity, shock sphere, pressure sensors, and pellet gun.

IV. EXPERIMENTAL METHOD

An over-all view of the apparatus used for the spherical-shock study is shown in Fig. 4. The low-pressure chamber (hereafter referred to as the shock cavity) is a cast-aluminum cylindrical resonant cavity which operates in the ultra-high frequency range. The shock cavity has a height of 44 cm and a diameter of 54.2 cm. It is fitted with 32 instrumentation portholes around the circumference and has openings for mounting the shock sphere, the pellet gun, and the vacuum system. The portholes permit the introduction of pressure sensors into the cavity and allow for radial variation in the position of the pressure sensors with respect to the center of the shock cavity.

The shock sphere, or high-pressure chamber, of the spherical-shock apparatus is a thin-shelled glass sphere with a diameter of 2 cm. The thickness of the sphere walls is about 0.04 cm, and each shock sphere weighs approximately one gram without the supporting stem. The tolerance allowed in manufacturing the spheres was ±5 percent in diameter. The spheres were hand blown from 6-mm-diameter Pyrex glass tubing, and each sphere was fitted with a supporting stem which was approximately 40 cm long. Each sphere was evacuated before being filled with air to a pressure of about 760 torrs. After the sphere was filled, it was sealed off from the supporting stem as shown in Fig. 5. This prevented gas in the stem from disturbing the flow when the glass diaphragm was ruptured. The stem, which serves as a rigid support for the shock sphere, passes through a special port in the cover plate of the shock cavity and permits a single glass sphere to be mounted in the center.

7

P781-114

Fig. 5. Typical shock sphere with supporting stem.

-35-8132

SHOCK SPHERE

PELLET LOADER

TOP COVER ASSEMBLY

SPRING

PLUNGER

BARREL

SAPPHIRE PELLET

TORSION SPRING
(loading position)

TORSION SPRING
(cocked)

LOADING ROD
(cocked)

TRIGGER BLOCK ASSEMBLY

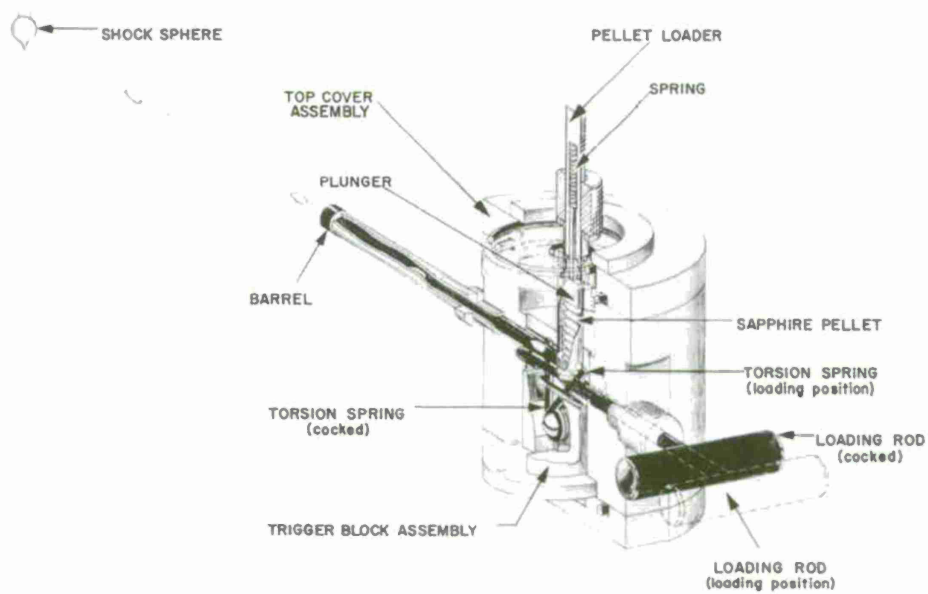LOADING ROD
(loading position)

Fig. 6. Schematic of pellet gun.

8

In operation, the shock sphere is broken by the impact of a 0.317-cm-diameter sapphire pellet fired from a spring-loaded vacuum-tight gun mounted at one end of the shock cavity. The gun is shown in position for operation in Fig. 4. Details of the firing mechanism are pictured in Fig. 6. The gun propels the conical or spherical pellet along the axis of the cylindrical shock cavity at a velocity of about 50 meters/sec. The exact value depends on the spring tension.

The method used to rupture the glass shock spheres proved to be quite satisfactory. The main advantage of using a pellet rather than a plunger, such as that used by others,[1,2] is that the ruptured sphere is less likely to be disturbed by the pellet. A double-exposure back-lighted spark shadowgraph of the rupture of an air-filled (750 torrs) sphere at an ambient pressure of 0.045 torr is shown in Fig. 7. The first exposure was made about 75 μsec after impact; the second exposure was made 475 μsec after impact. On impact (or soon thereafter) the sphere cracked extensively (see Fig. 7). As shown in the figure, a small "umbrella" from the sphere remained on the stem. The umbrella and stem will probably affect the formation of the shock wave and the issuance of gas from the ruptured sphere. The tip shown at the lower side of the sphere was not a part of the shock spheres which were used in obtaining the data reported in the succeeding sections of this report. Shadowgraph records showed that the tip usually came off as a sizeable glass fragment. The end of a pressure sensor can be seen in the lower left corner of Fig. 7. The spherical sapphire pellet can also be seen in the photograph.

Ammonium dihydrogen phosphate (ADP) pressure transducers were used to obtain pressure records of the flow field. These pressure sensors are modified Massa MK-107 piezoelectric microphones which are 0.635 cm in diameter. The sensor is mounted at the stagnation point of a flat-nosed metal probe which has an outer housing diameter of 1.270 cm and an over-all length of 46 cm. The instrument probe with electronics has a rise time of approximately 5 μsec. It is capable of responding to rapid changes in pressure, such as those associated with shock waves. A dynamic calibration of the pressure sensors yielded a sensitivity of 4.1 mv/torr. These calibration experiments were carried out in conventional shock tubes with the sensitive face of the pressure probes mounted parallel and normal to the free-stream flow. Details of the calibration experiments and a description of the theory of operation and performance of piezoelectric devices are given by Kornegay and Fridman.[9]

Five pressure sensors were used in performing the spherical shock studies. Other equipment included linear amplifiers with a 60-db dynamic range and a Model 501 Alphatron gauge.

In a typical experiment, an air-filled shock sphere was positioned at the center of the shock cavity, and one or more of the five available pressure sensors were placed at selected circumferential and radial positions in the cavity. When several probes were used simultaneously, they were arranged so as to minimize interference with the shock wave and between probes. The flat face of the pressure probes was normal to the spherical shock wave and the velocity of the contact surface. After the pellet gun was loaded, the shock cavity (including the interior of the gun) was pumped down to a pressure of less than 10^{-3} torr. The shock cavity was then filled to the desired ambient pressure, between 0.015 and 5.0 torrs. When the gun was fired, the sapphire pellet was projected along the cavity axis, impacted with, and ruptured the glass diaphragm. The subsequent main shock wave and the contact surface were detected by the pressure sensors. Each sensor's output was amplified and recorded on a Tektronix 555 oscilloscope. Typical responses of pressure sensors are shown in Fig. 8.
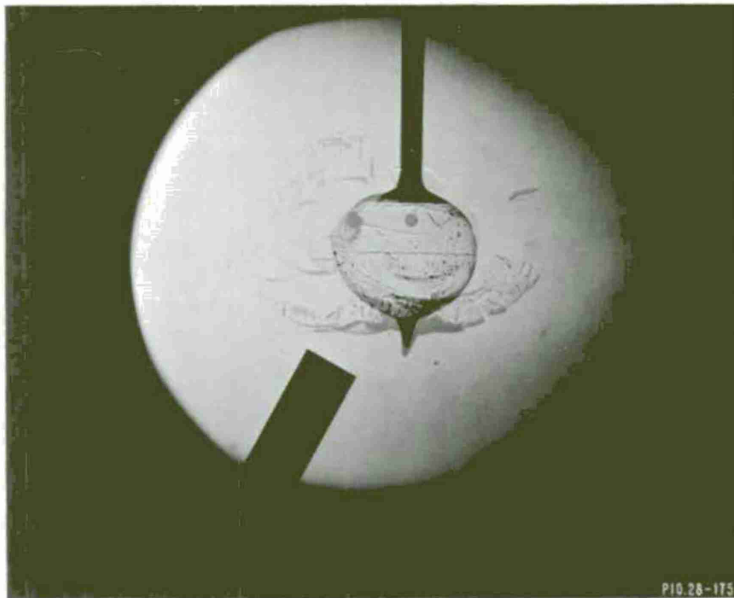
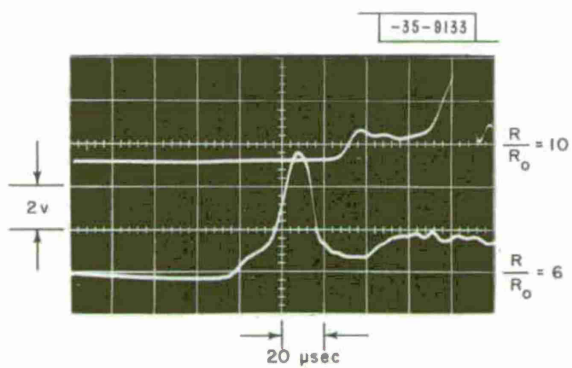Fig. 7. Photograph of shock sphere 75 μsec and 475 μsec after impact of pellet.

Fig. 8. Response of two pressure probes to a spherical shock wave and contact surface. Initial pressure = 0.050 torr.

10

V. METHOD OF DATA ANALYSIS

In the flow field resulting from the rupture of an isothermal sphere of gas at a pressure higher than the ambient pressure, the pressure-time history of a gas element at a location $R(R > R_o)$ is shown in Fig. 2 (curve labeled "spherical shock"). The pressure at location R suddenly jumps to a peak value of pressure P_2 when the shock wave arrives. The pressure immediately begins to decay, following a pressure history such as that shown in the figure.

The pressure sensor (ADP crystal) develops polarization charge when subjected to an abrupt pressure change such as that indicated in Fig. 2. This charge distributes itself over the capacitance which is in parallel with the pressure sensor. Consequently, the amplitude of the voltage appearing at the amplifier input is directly proportional to the applied pressure change, i.e.,

$$\Delta V = K \Delta P \tag{6}$$

where K, the constant of proportionality, has been determined by Kornegay and Fridman[9] in a series of dynamic calibration experiments. Its value is 4.1 mv/torr.

In the experiments reported here, the face of the pressure sensor was oriented normal to the free-stream streamlines. Hence, the pressure jump which one obtains from Eq. (6) and the measured voltage jump is $P_t - P_1$, where P_t is the impact pressure, and P_1 is the ambient or preshock pressure. The measured pressure jump decreases to zero in about 110 μsec. The time dependence of the pressure is discussed in Sec. VI-C.

The impact pressure is related to properties of the free-stream flow via the adiabatic isentropic expansion equation

$$\frac{P_t}{P_1} = (1 + \frac{\gamma - 1}{2} M_2^2)^{\gamma/\gamma - 1} \frac{P_2}{P_1} \tag{7}$$

for subsonic flow ($M_2 < 1$), and via the Rayleigh-Pitot relation

$$\frac{P_t}{P_1} = \left[\frac{(\frac{\gamma + 1}{2} M_2^2)^\gamma}{\frac{2\gamma}{\gamma + 1} M_2^2 - \frac{\gamma - 1}{\gamma + 1}} \right]^{1/\gamma - 1} \frac{P_2}{P_1} \tag{8}$$

for supersonic flow ($M_2 > 1$), where P_t and P_2 are the impact and free-stream pressures, respectively, γ is the specific heat ratio which is assumed to be constant, and M_2 is the free-stream or flow Mach number which is related to the free-stream pressure by

$$M_2 = \frac{(P_2/P_1 - 1)}{\gamma} \left[\frac{\gamma - 1}{2\gamma} \frac{P_2}{P_1} \left(\frac{\gamma + 1}{\gamma - 1} + \frac{P_2}{P_1} \right) \right]^{-1/2} . \tag{9}$$

The flow Mach number behind a normal shock wave or immediately behind a spherical shock wave is related to the shock Mach number M_s by

$$M_2 = \frac{2(M_s^2 + 1)}{[(2\gamma M_s^2 - \gamma + 1)(\gamma M_s^2 - M_s^2 + 2)]^{1/2}} . \tag{10}$$

Equations (7) through (10) have been used to prepare plots of P_t/P_1 and P_2/P_1 vs M_s which are given in Fig. 9. These graphical representations have been used in obtaining the experimental values of shock Mach number, flow Mach number, and free-stream pressure that are presented in the following sections of this report.
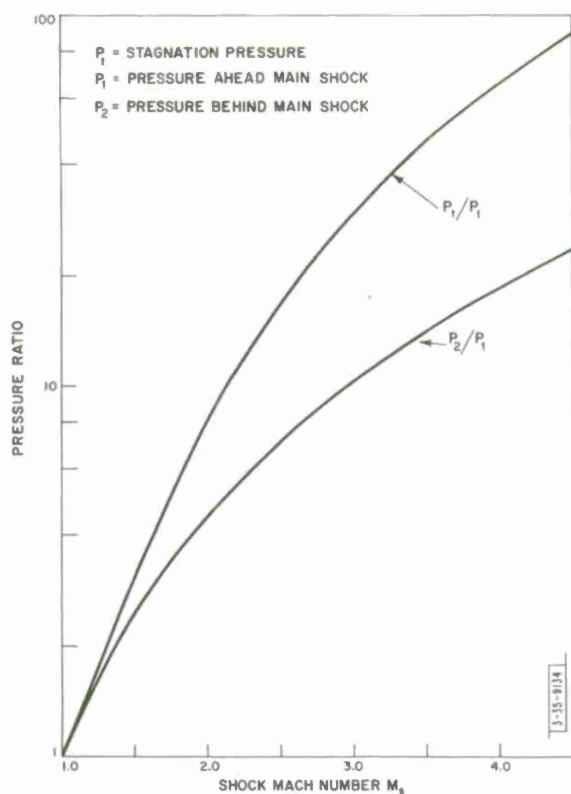
Fig. 9. Free-stream and impact pressure ratios as a function of shock Mach number.

VI. EXPERIMENTAL RESULTS AND DISCUSSION

A. Shock Wave Symmetry and Sphericity

The symmetry and sphericity of the shock wave with respect to the center of the shock cavity were investigated by observing the intensity of pressure signals and the time of arrival of the main shock wave at several probes equidistant from the geometric center of the shock cavity. Four pressure sensors were placed in a plane which is perpendicular to the cavity axis and which passes through the cavity center. The probes were arranged so that the maximum circumferential separation of any two probes was 120 degrees and the minimum was 30 degrees ("arrangement A"). In "arrangement B," the set of four probes was placed in the plane that is perpendicular both to the plane of arrangement A and to the stem of the shock sphere, and includes the axis of the shock cavity. The maximum separation between any two adjacent probes was 115 degrees and the minimum was 65 degrees.

With the four probes always equidistant from the cavity center, their radial position was varied, and at each position, measurements were made on the flow resulting from the bursting of a shock sphere. In particular, the relative time of arrival of the main shock wave and the contact surface at each probe was recorded. This phase of the study was carried out at an ambient air pressure of 0.060 torr, using 2-cm-diameter air-filled (750 torrs) shock spheres.

Experiments performed with the set of four probes located at several positions between $R/R_o = 5$ and 24 (R_o is the radius of the unruptured glass spheres) show that at a given radius the maximum deviation in position of the spherical shock wave with respect to its mean position is ±4 percent. This result shows the combined effects of any nonspherical features of the shock wave, asymmetry in the shape of the unruptured shock sphere, and failure to position the shock

12

sphere at the exact geometrical center of the shock cavity. Since the deviation in apparent symmetry is the same at all radii, we assume that the observed effect is associated with the shock source (the shock sphere). Irregularities in the shock wave surface would tend to smooth out with increasing distance. The more reasonable of the two remaining explanations is that the shock sphere is not positioned at the exact geometrical center of the cavity initially. This is probably because the shock sphere was not positioned symmetrically on its stem. It is reasonable for a 2-cm hand-blown glass sphere to have its center lie as much as 0.4 mm off the axis of the stem on which it is blown. Hence, the experiments have not yielded results which suggest that shock waves formed as a result of shattering glass spheres at low ambient densities are not spherical.
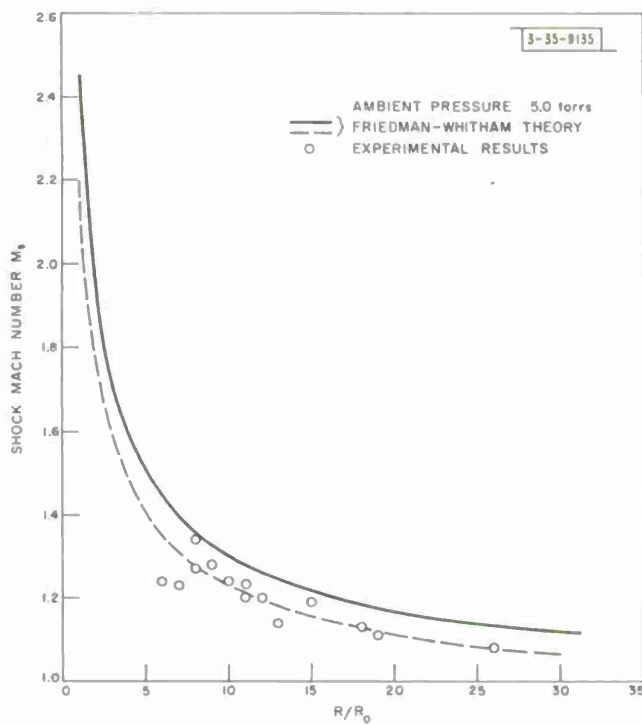
B. Strength of the Main Shock Wave

The shock strength has been measured as a function of the shock radius at seven values of the ambient pressure between 0.015 and 5.0 torrs. (Here the Mach number is taken to be a measure of the shock strength.) At each pressure, the radial position of each of four pressure sensors was varied. This permitted one to obtain data from which a measure of the shock strength as a function of the shock radius could be deduced. The magnitude of the initial rise on the pressure-history record provided by each pressure sensor is a measure of the impact pressure, which can be readily related to the free-stream parameters immediately behind the shock wave and to the speed of the shock wave itself (see Sec. V). Results of the analysis of the oscillogram records of these experiments, using Eqs. (6), (7), (8), and (10), are shown for various ambient pressures in Fig. 10(a-g). The solid line on each figure is determined from the Friedman-Whitham theory for spherical blasts (Sec. II-C). In using this theory, it was assumed that the theoretical shock strength at $R/R_o = 1$ is related to the initial pressure ratio across the glass diaphragm by Eq. (5). The implication here is that the shock formation is ideal, i.e., that the diaphragm is removed instantaneously and that the energy lost in accelerating glass fragments is negligibly small. These assumptions will be considered further in Sec. VII.

The strength of the main shock wave has also been measured at 0.04 and 0.10 torr by recording the times of arrival of the shock wave at several probes located at different radial positions. In these experiments, one obtains an average Mach number from measurements with pairs of probes which are separated by 2 cm in the radial direction. The Mach numbers M_T obtained in this way are plotted against nondimensional radii in Fig. 11(a-b). The theoretical curve (solid line) on these figures was also calculated with the Friedman-Whitham theory for spherical blasts.
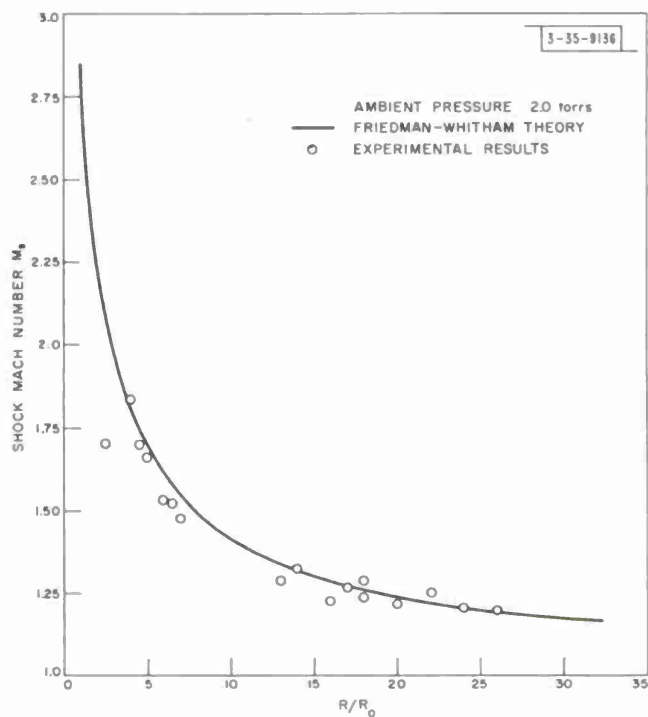
C. Secondary Shock Wave

The interesting phenomenon of a secondary shock wave (see Sec. III) is known to appear in spherical flows. In the work reported here, observations have been made which indicate that a secondary shock wave is a part of the flow field. However, no attempt has been made to study it extensively.

In experiments which were carried out at 5.0 torrs, the pressure records from pressure probes located at $R/R = 5$ and 6 showed a pressure jump occurring approximately 400 μsec after the main shock wave had arrived. The second signal on these records was about one-half the height of that for the main shock wave and was probably produced by the secondary shock wave.

AMBIENT PRESSURE 5.0 torrs
FRIEDMAN-WHITHAM THEORY
O EXPERIMENTAL RESULTS

SHOCK MACH NUMBER M_s

R/R_0

(a) $P_4/P_1 = 130.$

AMBIENT PRESSURE 2.0 torrs
FRIEDMAN-WHITHAM THEORY
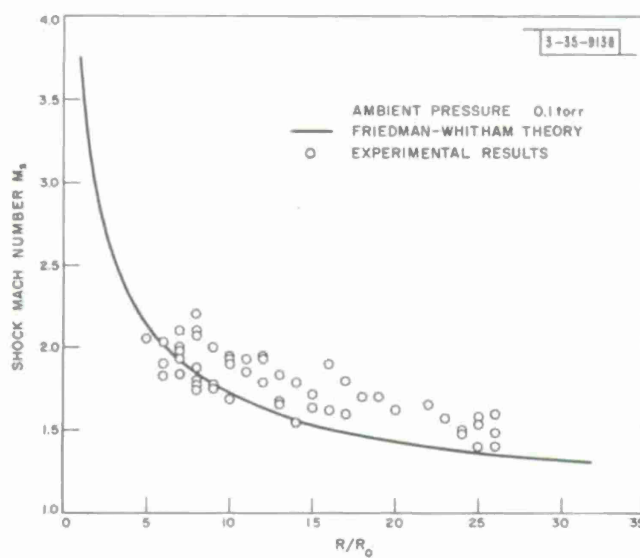O EXPERIMENTAL RESULTS

SHOCK MACH NUMBER M_s

R/R_0

(b) $P_4/P_1 = 425.$

Fig. 10(a-g). Variation of shock Mach number with shock radius
for various ambient pressures.

14

(c) $P_4/P_1 = 1.7 \times 10^3$.
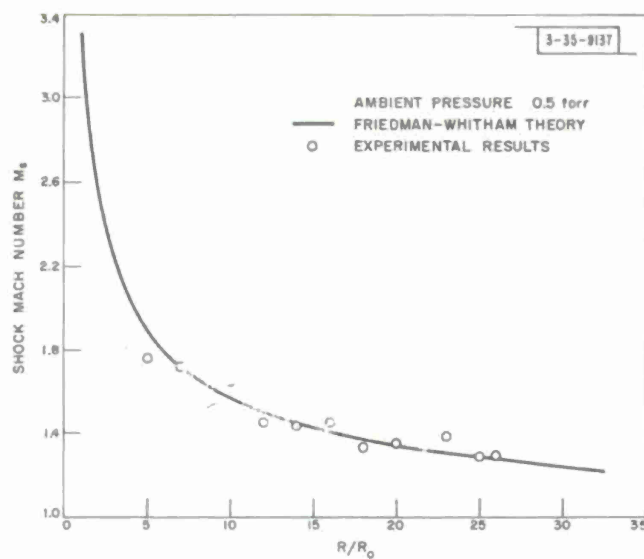
(d) $P_4/P_1 = 7.5 \times 10^3$.

(e) $P_4/P_1 = 1.3 \times 10^4$.

Fig. 10. Continued.

15

(f) $P_4/P_1 = 1.9 \times 10^4$.

(g) $P_4/P_1 = 5.0 \times 10^4$.

Fig. 10. Continued.

16
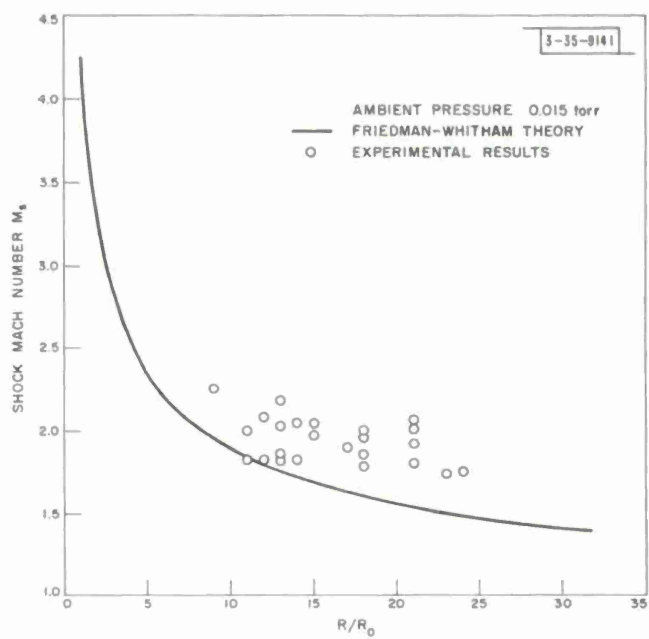
(a) $P_4/P_1 = 1.9 \times 10^4$.
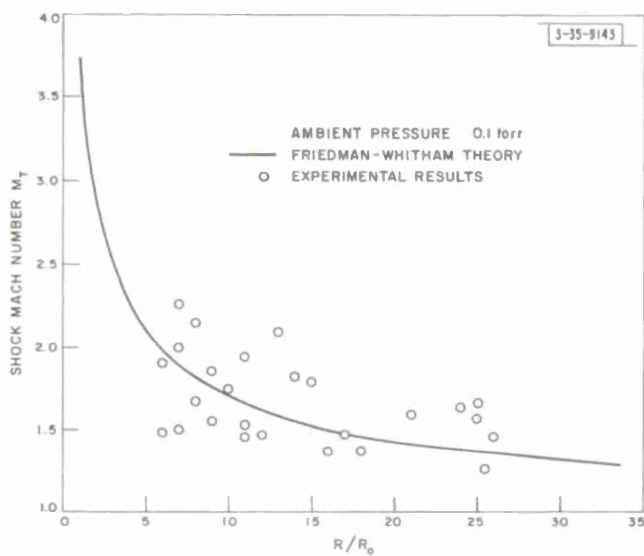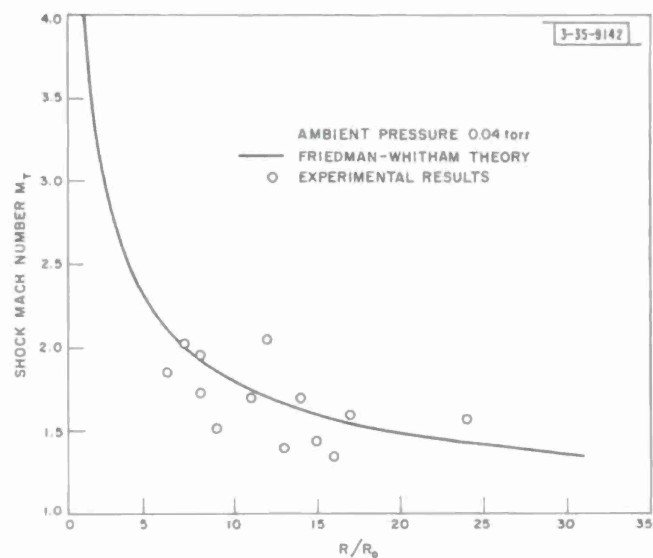
(b) $P_4/P_1 = 7.5 \times 10^3$.

Fig. 11(a–b). Average Mach number based on shock transmit time as a function of shock radius.
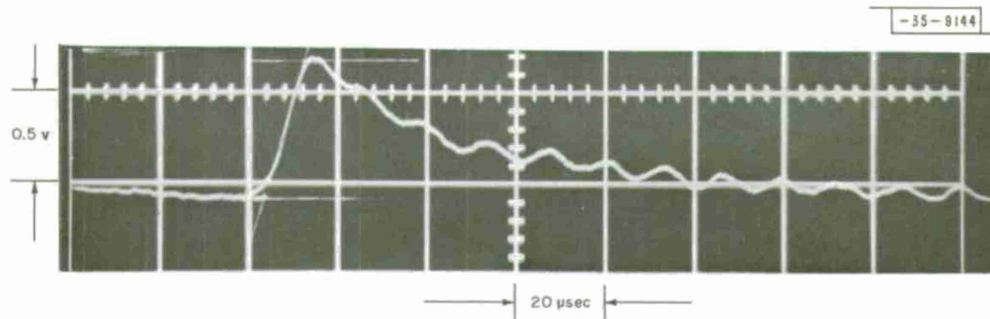
Fig. 12. Response of pressure probe to spherical shock wave in absence of a contact surface. Initial pressure = 0.1 torr. $R/R_o = 23$.
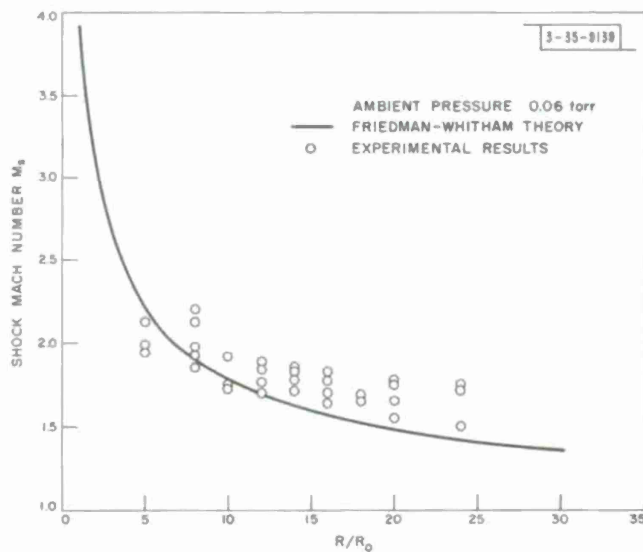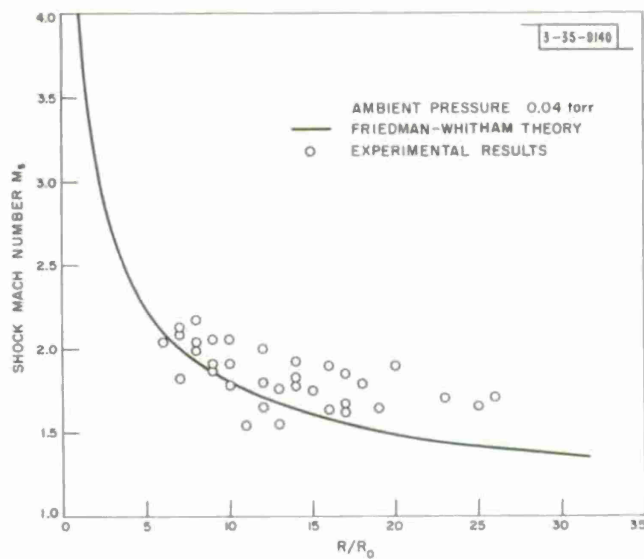
TABLE I				
CONTACT SURFACE DATA				
Pressure	Computed Maximum Radius	Maximum R/R_o Contact Surface Observed	Minimum R/R_o No Contact Surface Observed	Lag Time for Contact Surface Arrival
5.0	5.3	5.0	6.0	20
2.0	7.2	7.0	8.5	20
0.5	11.5	10.0	12.0	20
0.1	19.6	18.0	19.0	80
0.06	23.2	24.0	–	90
0.04	26.5	26.0	–	60
0.015	36.8	24.0	–	80

18

D. Contact Surface

Under certain conditions, it has been observed that the pressure pulse which results from the main shock wave is followed closely by a second pressure jump (see Fig. 8). The behavior of the second signal was investigated by varying the pressure and the radial probe position and observing any change in the separation of the two signals, and by varying the ambient pressure in the shock cavity to see if there were a maximum radius at which the second signal could be detected. The results of these studies were that: (1) the shock wave signal and the second signal tended to separate from each other with increasing distance (e.g., Fig. 8); (2) at pressures of 0.1 torr or more, a radial position could be found where the second signal apparently did not occur (e.g., see Fig. 12); and (3) the relative magnitudes and arrival times of the second signal at several equidistant pressure sensors were not nearly so reproducible as they were for the main shock wave signal. On the basis of these facts, it was concluded that the second signal on oscillogram records, such as that shown in Fig. 8, is caused by the arrival of the gas interface (contact surface) at the pressure sensor. It could not possibly be caused by the second shock wave or any other known feature of the flow system which arises in the formation of spherical shock waves.

If the ambient pressure is low, the gas initially contained in the glass shock sphere moves out to occupy a large volume when the shock sphere is broken. In fact, the sphere gas expands until its pressure is approximately equal to the ambient pressure. In Table I, the measured final radius of the sphere gas is compared with the maximum theoretical radius, calculated under the assumption that the sphere gas undergoes an isothermal expansion and that there is no diffusion. Adiabatic expansion calculations yield final radii about one-half as large as those for isothermal expansion. Measurements and calculations are for 2-cm-diameter spheres of air. The maximum radius at which the contact surface was detected is given in column 3, and the minimum radius at which it was not detected is given in column 4. The gap in the data exists only because no attempt was made to make a more definite establishment of the location of the final contact surface radius. Column 5 gives the difference in shock and contact surface arrival at the radius R/R_o given in column 3. It should be noted that the maximum radial dimension of the shock cavity is 27.2 cm. Therefore, it becomes very difficult to differentiate between the arrival of the contact surface and the reflected shock wave at large radii.

As mentioned, the experiments with the pressure sensors equidistant from the shock cavity center indicated that the contact is quite irregular in shape. The experiments also showed that the shape of the contact surface is not nearly so reproducible as the spherical shock wave is from one experiment to the next. Since the initial escape of the gas from various circumferential positions of the shock sphere is affected to varying degrees by the fragments of the ruptured glass sphere, these observations on the contact surface are not at all surprising.

The formation of a contact surface is a characteristic feature associated with the production of shock waves. The contact surface is the interface between the two gases which were initially on either side of the glass diaphragm. The temperatures and the densities on the two sides of the contact surface may be different, but it is necessary that the fluid velocity and pressure be the same. In practice, however, the spreading of the contact surface because of heat conduction and diffusion will cause limited departure from these requirements.

A cursory inspection of the statements of the last paragraph might lead one to conclude that the arrival of the contact surface at an impact probe would not result in a significant change in
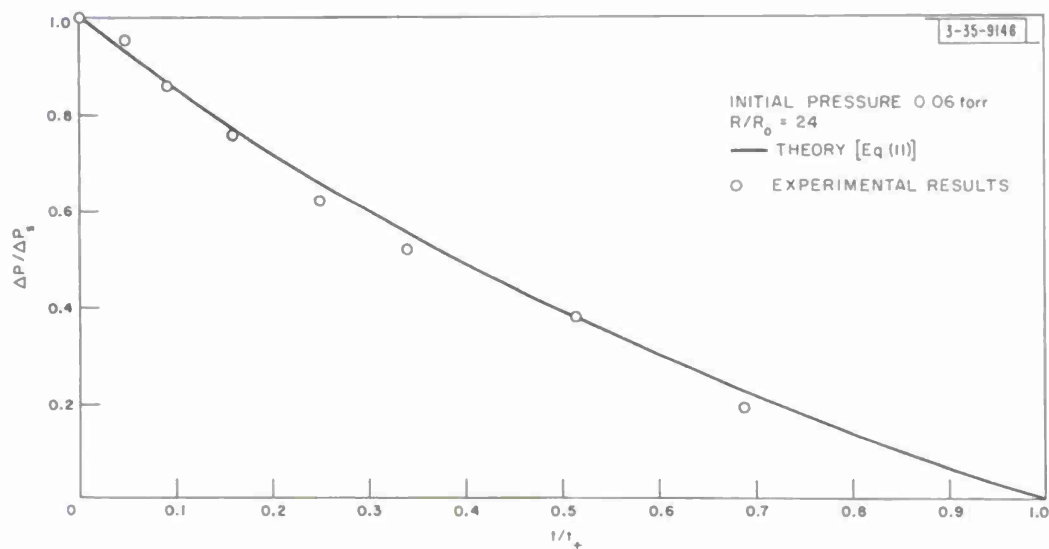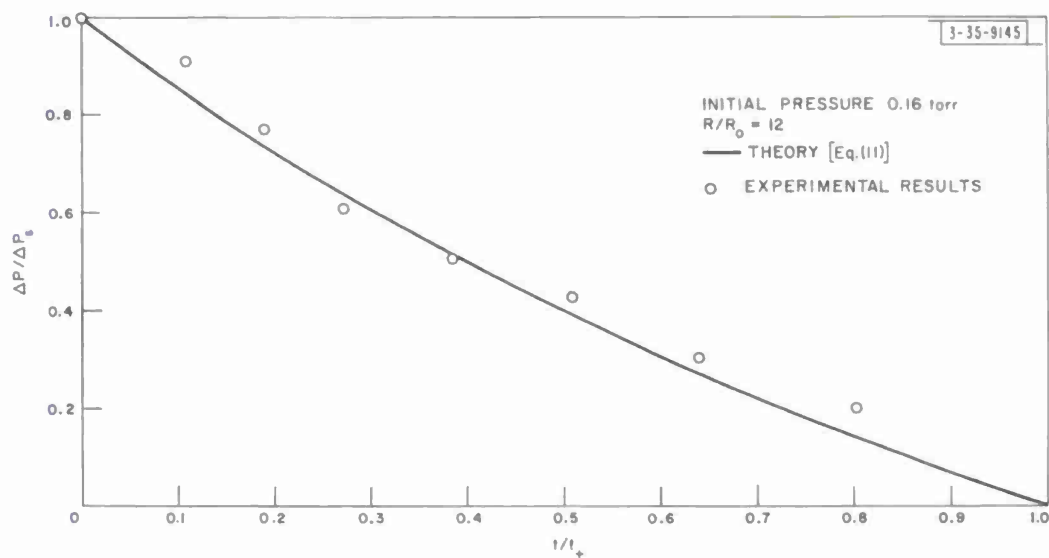
Fig. 13(a-b). Decay of spherical shock overpressure.

the pressure signal. However, close inspection of the equations (see Sec. V) which govern the response of an impact probe with its face oriented normal to the free-stream flow indicates that a contact surface should give rise to a pressure signal, even when air is on both sides of the interface. The gas on the expansion side of the contact surface is at a lower temperature than the gas on the compression side. This means that the expanded gas will have a higher flow Mach number than the compressed gas. Consequently, the measured impact pressure is higher on the expansion side of the contact surface.

E. Time Dependence of Pressure

The excellent low- and high-frequency response characteristics of the pressure sensors described in Sec. IV make it possible for one to use the sensors to follow not only the initial pressure pulse, but also any subsequent change in pressure that occurs within several milliseconds.

At a particular radius in the shock cavity, a given fluid element is at ambient pressure P_1 prior to the arrival of the main shock wave. The gas is raised to a higher pressure P_2 as a result of being traversed by the shock wave. After the spherical shock wave passes, the pressure decreases with time. The time dependence of the pressure jump produced by the shock wave can be approximated by[10]

$$\frac{\Delta P}{\Delta P_S} = \left(1 - \frac{t}{t_+}\right) \exp\left[\frac{-\alpha t}{t_+}\right] \tag{11}$$

where ΔP_S $[\Delta P_S = (P_2 - P_1)/P_o]$ is the shock overpressure, ΔP is the overpressure at any time t after the shock arrives, and t is a measure of the duration of the positive phase of overpressure. The reference pressure P_o is taken to be 1 atmos. The coefficient α is given by

$$\alpha = 0.5 + \Delta P_S \quad . \tag{12}$$

This simple exponential dependence of overpressure is satisfactory for ΔP_S less than one. Its derivation is based on a blast profile similar to that from a point source.

Although Eq. (11) was originally derived for a point-source blast profile, it can be expected to be applicable to finite source experiments when the overpressures have reached point-source values.[10] In order to examine this proposition, experiments were performed with 2-cm shock spheres filled with air at several ambient pressures between 0.04 and 0.5 torr. The closeness of the second pressure signal (contact surface) behind the spherical shock wave made it difficult to obtain extensive data over this pressure range and at the shock wave radii accessible in the shock cavity.

A typical oscillogram of the pressure (impact) history is shown in Fig. 12. At low flow Mach numbers, the free-stream pressure history will closely parallel the impact pressure history. The two can be exactly related through the equations given in Sec. V. The time dependence of the free-stream pressure (i.e., the pressure in state 2 of Fig. 3) at a given shock radius is an interesting feature of the flow behind spherical shock waves. In Fig. 13(a-b), the free-stream overpressure is plotted as a function of time after passage of the shock wave for several experiments. The solid lines are plots of Eq. (11). In these figures, the overpressure is normalized with respect to the peak overpressure, and the time is normalized with respect to the duration of the positive overpressure pulse. The experimentally determined duration of the positive overpressure pulse for experiments with air-filled spheres was approximately 110 μsec. The peak overpressures were calculated from the pressure records by using the Rayleigh-Pitot and Rankine-Hugoniot relations given in Sec. V.

F. Shock Thickness

It is possible to obtain an estimate of the thickness of the spherical shock wave from the rise time of the measured pressure signal. Usually the shock thickness L is defined in terms of the density profile through the shock wave.[11] Here, it is defined in terms of the measured pressure profile. The difference in definitions will not be of significant consequence at low shock wave velocities.

The shock thickness was found by taking the product of the measured rise time and the speed (Mach number times sound speed) at which the shock wave moved past the face of the pressure sensor. The rise time was obtained by extrapolating the maximum slope of the pressure pulse to the initial and final states of the event and measuring the time between the points of intersection. The rise times obtained in this manner ranged from 4μsec at 5.0 torrs to about 30μsec at 0.015 torr.
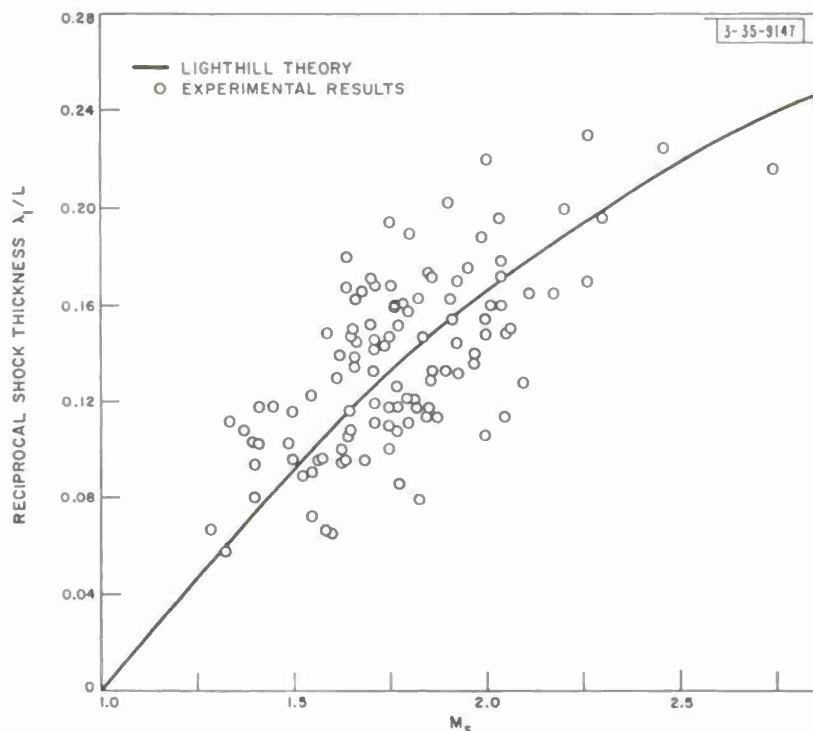
Fig. 14. Variation of experimental and theoretical shock thickness with shock Mach number.

The shock thickness was computed only for those pressure records which had a rise time at least twice as large as the response time (5μsec) of the pressure sensor system. This means that all shock thickness data are for experiments at pressures of 0.10 torr or less. The reciprocal of the shock thickness (in units of mean free paths of the gas ahead of the shock wave) is plotted as a function of the shock Mach number in Fig. 14. The solid line was calculated from an equation by Lighthill,[12] which gives an upper bound for the reciprocal shock thickness.

Lighthill's equation is derived from considerations of energy dissipation. In the derivation, he starts with the equation for entropy production in the shock wave and arrives at the following relation for the shock thickness:

$$L \geqslant \frac{(1.33\mu_2 + \mu_2') \frac{V_2^2}{T_1} + \left(\int_{T_1}^{T_2} k^{1/2} \frac{dT}{T}\right)^2}{\rho_1 U \Delta S} \tag{13}$$

where μ, μ', V, T, ΔS, ρ, U, and k denote shear viscosity, bulk viscosity, free-stream veloc-
ity, temperature, entropy change across the shock, density, shock wave velocity, and thermal
conductivity, respectively. The subscript 1 denotes conditions ahead of the shock wave, and the
subscript 2 denotes conditions behind the shock wave. In calculating the shock thickness from
Eq. (13), μ is assumed to be proportional to $T^{0.8}$. As shown in Fig. 14, the experimental values
of shock thickness are within a factor of 1.5 of the values predicted by the Lighthill equation.
Since no significant relaxation effects occur in low-velocity shock waves, this fair agreement
does not come as a surprise.

VII. COMPARISON OF SHOCK MACH NUMBER WITH THEORY

Examination of Fig. 10(a-g) shows that when the diaphragm pressure ratio P_4/P_1 is greater
than about 500, and when effects of viscous and rarefied phenomena (see Sec. VIII) are absent
from the probe measurements, there is excellent agreement [see Fig. 10(b and c)] between the
Friedman-Whitham theory and the experimental results obtained from impact pressure measure-
ments. Also, when the Mach numbers are determined from the time of flight of the shock be-
tween two stations, good agreement is obtained between theory and experiment [see Fig. 11(a-b)]
in the ambient pressure region where viscous and rarefied gas phenomena affect impact pres-
sure measurements. In Sec. VIII, it will be shown that after certain corrections to the data, the
experimental results at 0.1, 0.06, 0.04, and 0.015 torr are also in good agreement with the sim-
plified theory of Friedman and Whitham.

The favorable comparison between theory and the experiments indicates that the weakening
of the main shock wave, as it moves out radially, is primarily caused by the increase in shock
surface area. On the other hand, this means that information about the flow behind the shock
wave, which reaches the shock by means of the positive characteristics, can be neglected in the
range of Mach numbers covered by these experiments.

The experimental data at 5.0 torrs ($P_4/P_1 = 130$) fall below the theoretical curve by approxi-
mately 5 percent [see Fig. 10(a)]. Because of the good agreement with theory of the 2.0- and 0.5-
torr data and the absence of rarefied gas effects at this pressure, these data could be expected
to be in agreement with theory. The initial Mach number (M at $R/R_0 = 1$) has to be decreased
by 10 percent in order for the theory to give the broken line through the data points of Fig. 10(a).
This means that approximately 50 percent of the shock driving energy was lost (i.e., used for
some purpose other than for driving the shock wave). This loss of energy can probably be attrib-
uted to the presence of glass particles from the sphere in the spherical flow field.

The total energy initially stored in the sphere is

$$E = nC_v T \tag{14}$$

where n is the number of moles of gas, C_v is the heat capacity per mole at constant volume,
and T is the temperature in degrees Kelvin. For the 2-cm-diameter sphere filled with air to
a pressure of 1 atmos at 300°K, the stored energy is 10^7 ergs. Making the very crude assump-
tion that 50 percent of this energy is consumed in accelerating all the fragments of the one-gram
sphere to a uniform velocity V, one computes a velocity of 32 meters/sec. This velocity for the

23

glass fragments is in fair agreement with several rough estimates of glass particle velocity which were made from shadowgraph records of ruptured glass spheres. Hence, the presence of glass particles in the flow field does provide a qualitative explanation for the adverse effect observed at the low initial pressure ratio (P_4/P_1 = 130). Unfortunately, measurements that would yield quantitative information on the size and velocity of glass particles in the flow field were not made.

Since the fraction of the total energy which is used in breaking and in accelerating glass particles should be nearly constant for a glass sphere of a given diameter, one would expect that as the pressure ratio P_4/P_1 across the unruptured glass diaphragm or the initial energy of the gas stored in the sphere is increased, the effect of the energy loss would decrease. A loss of 5 × 10^6 ergs, which is the amount of energy lost at P_4/P_1 = 130, at P_4/P_1 = 425 [Fig. 10(b)] is 14 percent of the total initial energy. This results in the initial Mach number and in the Mach number at radii greater than R_o being lowered by 1.4 percent or less. The effect is even less for higher initial pressure ratios. Consequently, the presence of glass particles in the flow field resulting from the rupture of the 2-cm-diameter spheres used in the work reported here does not affect the shock strength, as long as the initial pressure ratio exceeds approximately 500.

VIII. LOW AMBIENT PRESSURE EFFECTS

Under ordinary conditions, the Mach number may be calculated from the ratio of impact pressure to ambient pressure using the mathematical relations given in Sec. V. It has long been recognized[13-15] that this ideal situation persists only as long as the gas pressure and density are sufficiently high, i.e., when the impact probe measurements are made in continuum flow. At low gas pressures, rarefied gas phenomena and viscous effects tend to cause the impact pressure to depart radically from the theoretical value for continuum flow. The extent to which the measured pressure is made to vary from the ideal impact pressure as given by Eq. (7) or (8) is a function of the flow Mach number, the shape of the pressure probe, and either the Reynolds or the Knudsen number. Viscous correction data for probes of various shapes can be found in the literature.[13-15] However, to the author's knowledge, such data are not available for blunt-faced pressure probes in low-pressure air.

The Knudsen number Kn is the basic parameter that indicates the degree of rarefaction of a gas. It is defined as Kn = λ/L, where L is the characteristic body dimension, and λ is the molecular mean free path. For the work reported here, L is taken to be the diameter of the pressure probe, which is 1.27 cm. The Knudsen number computed for the flow immediately behind the spherical shock wave varies from 0.0005 at 5.0 torrs to 0.2 at 0.015 torr.

The Knudsen number can be used to make a rough division of gas dynamics into the following regimes:[16]

Free molecule flow	Kn > 5
Transition flow	5 > Kn > 0.1
Slip flow	0.1 > Kn > 0.01
Continuum flow	Kn < 0.01

This classification of flow regimes indicates that the measurements reported here span at least two flow regimes — the continuum and the slip regimes.

Viscous effects and/or rarefied gas phenomena usually cause the measured impact pressure to exceed the ideal impact pressure when the measurements are made in slip, transition, or free

molecule flow. The ratio of the measured to ideal impact pressure, $P_{t, exp}/P_{t, ideal}$, is usually used to indicate the extent to which the measured pressure deviates from the ideal impact pressure which is computed from the Rayleigh-Pitot relation or the adiabatic isentropic relation. The fact that the experimental Mach numbers in the continuum flow regime [see Fig. 10(b and c)] are in good agreement with the Mach numbers computed from blast wave theory indicates that the viscous correction factor, $P_{t, exp}/P_{t, ideal}$, is approximately equal to one over the complete Mach number range. At the low pressures [see Fig. 10(d, e, f, and g)], a correction factor is needed. No correction is needed for the 0.04- and 0.1-torr data of Fig. 11(a-b), because the Mach numbers are determined from the time of travel of the shock wave between the probes. The viscous factors given in column 4 of Table II represent the values of $P_{t, exp}/P_{t, ideal}$ that are needed to bring the measured Mach numbers into essential agreement with the Friedman-Whitham blast theory. Since the factor is a function of pressure (Knudsen number) and Mach number, the table has been limited by including the correction factor at a single Mach number (M_2 value at $R/R_o = 15$) for each pressure. The corresponding flow Mach number and Knudsen number are given in columns 2 and 3, respectively. In column 5, the free molecule flow values of $P_{t, fmf}/P_{t, ideal}$ are given. The latter values were computed for the blunt-faced probes used in these experiments from an equation given by Enkenhus.[17] Although the equation was derived for computing the viscous factor for the orifice type probe, it can be applied to the blunt-faced probe by setting the orifice opening equal to zero. Since the correction factor is expected to increase with rarefaction of the medium, the $P_{t, fmf}/P_{t, ideal}$ value calculated from the Enkenhus formula is an upper limit for viscous correction for a given probe at the specified Mach number and Knudsen number.

TABLE II

COMPARISON OF VISCOUS CORRECTION FACTORS OBTAINED
FROM EXPERIMENTAL DATA AT $R/R_o = 15$ WITH VALUES COMPUTED
FROM THE ENKENHUS FORMULA

Pressure (torr)	Knudsen Number (λ/L)	Flow Mach Number (M_2)	$P_{t, exp}/P_{t, ideal}$	$P_{t, fmf}/P_{t, ideal}$ *
0.015	0.135	0.745	1.67	1.84
0.04	0.053	0.690	1.38	1.80
0.06	0.036	0.665	1.32	1.79
0.10	0.022	0.630	1.25	1.76
0.50	0.0049	0.525	1.00	1.67
2.0	0.0014	0.410	1.00	1.56
5.0	0.0006	0.300	0.95	1.42

* This ratio was computed from the Enkenhus formula for free molecular flow.[17]

IX. CONCLUSIONS

This work has demonstrated that a reproducible spherical shock wave can be produced by suddenly rupturing a thin-walled 2-cm-diameter spherical diaphragm which separates a gas approximately at atmospheric pressure from a surrounding gas at a pressure between 0.015 and 5.0 torrs. At these low pressures, the spherical flow field exhibited all the main features that have been observed by investigators working at higher ambient and shock sphere pressures.

Data obtained from impact pressure records of the flow have shown that the main shock wave's strength, thickness and rate of radial decay, and the time history of the shock overpressure are in fair to excellent agreement with existing theories. A quantitative comparison of the experimental data on shock decay with the approximate spherical shock theory of Friedman and Whitham has shown that the shock strength decreases primarily as a result of the increase in the shock surface area as the shock radius increases.

It was observed that the strength of the main shock wave is not affected by the presence of glass particles in the flow field, as long as the initial pressure ratio across the glass diaphragm is about 500 or more. At lower pressure ratios, the presence of glass particles tends to decrease substantially the amount of energy that is initially available for driving the shock wave. The shock strength is then lower than one would predict from theory.

The investigation has shown that, at Knudsen numbers corresponding to the slip and transition flow regimes, viscous and rarefied gas effects cause the measured impact pressure to deviate from the correct pressure. The correction factors that are necessary to account for the deviation in impact pressure have been determined from the data and were found to be reasonable in that they are less than the corresponding free molecule flow correction factor would be.

REFERENCES

1. D.W. Boyer, H.L. Brode, I.I. Glass and J. Hall, UTIA Report No. 48, Institute of Aerophysics, University of Toronto (January 1958).

2. D.W. Boyer, UTIA Report No. 58, Institute of Aerophysics, University of Toronto (November 1959).

3. I.I. Glass, Can. Aeronaut. J. 7, 109 (1961).

4. J. von Neumann and R. D. Richtmyer, J. Appl. Phys. 21, 232 (1950).

5. H.L. Brode, Report P-1933, The RAND Corporation (February 1960).

6. G.B. Whitham, J. Fluid Mech. 4, 337 (1958).

7. R.F. Chisnell, J. Fluid Mech. 2, 286 (1957).

8. M.P. Friedman, J. Fluid Mech. 11, 1 (1961).

9. W.M. Kornegay and J.D. Fridman, "Calibration of a Pressure Sensor for Measurements in Continuum and Rarefied Gas Flows," Technical Report 379, Lincoln Laboratory, M.I.T. (8 February 1965).

10. H.L. Brode, J. Appl. Phys. 26, 766 (1955).

11. J.N. Bradley, Shock Waves in Chemistry and Physics (Wiley, New York, 1962), Chap. VI.

12. M.J. Lighthill in Surveys in Mechanics, G.K. Batchelor, ed. (Cambridge University Press, London, 1956), pp. 294-297.

13. F.S. Sherman, Technical Note 2995, National Advisory Committee for Aeronautics (September 1953).

14. A.B. Bailey, Technical Report No. AEDC-TDR-62-208, Arnold Engineering Development Center, AFSC, Tennessee (November 1962).

15. S.I. Kosterin, N.I. Yushchenkova, N.T. Belova and B.D. Kamayev, Inzh.-Fiz. Zh. 5, 16 (1962).

16. G.N. Patterson, Can. Aeronaut. J. 7, 13 (1961).

17. K.R. Enkenhus, UTIA Report No. 43, Institute of Aerophysics, University of Toronto (January 1957).

DOCUMENT CONTROL DATA - R&D

(Security classification of title, body of abstract and indexing annotation must be entered when the overall report is classified)

1. ORIGINATING ACTIVITY *(Corporate author)*	2a. REPORT SECURITY CLASSIFICATION
Lincoln Laboratory, M.I.T.	Unclassified
	2b. GROUP

3. REPORT TITLE

Production and Propagation of Spherical Shock Waves at Low Ambient Pressures

4. DESCRIPTIVE NOTES *(Type of report and inclusive dates)*

Technical Report

5. AUTHOR(S) *(Last name, first name, initial)*

Kornegay, Wade M.

6. REPORT DATE	7a. TOTAL NO. OF PAGES	7b. NO. OF REFS
26 January 1965	32	17

8a. CONTRACT OR GRANT NO.	9a. ORIGINATOR'S REPORT NUMBER(S)
AF 19(628)-500	Technical Report 375
b. PROJECT NO. ARPA Order 600	
c.	9b. OTHER REPORT NO(S) *(Any other numbers that may be assigned this report)*
d.	ESD-TDR-65-35

10. AVAILABILITY/LIMITATION NOTICES

11. SUPPLEMENTARY NOTES	12. SPONSORING MILITARY ACTIVITY
	Advanced Research Projects Agency, Department of Defense

13. ABSTRACT

An experimental investigation has been made of the spherical shock waves produced when 2-cm-diameter thin-walled glass spheres, which have been filled with air at a pressure of about 760 torrs, are burst in an ambient environment of dry air pressures ranging from 0.015 to 5.0 torrs.

Piezoelectric pressure transducers were used to measure the rate of decay of the spherical-shock Mach number with increasing radius. A comparison of the experimentally observed shock Mach numbers with those predicted from calculations based on an approximate theory by Friedman and Whitham shows that the two are in good agreement. Shock overpressures and shock thickness determined from impact pressure records are in fair agreement with existing approximate theories.

The effect of glass particles on the flow field was found to be important when the initial pressure ratio across the glass diaphragm is below 500. At low pressures, viscous and rarefied flow phenomena tend to cause the measured impact pressure to depart radically from the theoretical value for continuum flow.

14. KEY WORDS

spherical shock waves	piezoelectric transducers
spherical flow fields	low-pressure effects
gas dynamics	